Applied Thermal Engineering 31 (2011) 3287–3300

Contents lists available at ScienceDirect

Applied Thermal Engineering

journal homepage: www.elsevier.com/locate/apthermeng

Key modeling issues in prediction of minor species in diluted-preheated combustion conditions

J. Aminian [a], C. Galletti [b], S. Shahhosseini [a,*], L. Tognotti [b,**]

[a] Department of Chemical Engineering, Iran University of Science and Technology (IUST), Tehran, Iran
[b] Dipartimento di Ingegneria Chimica, Chimica Industriale e Scienza dei Materiali, Università di Pisa, Pisa, Italy

ARTICLE INFO

Article history:
Received 22 February 2011
Accepted 6 June 2011
Available online 13 June 2011

Keywords:
Flameless
Turbulence-chemistry interaction
Combustion model
Shear layer
Scalar fluctuation

ABSTRACT

A numerical investigation of a jet in hot coflow (JHC) burner emulating Moderate or Intense Low-oxygen Dilution (MILD) combustion is carried out in order to understand key modeling issues for such three stream problem. Favre-averaged Navier–Stokes (FANS) equations were solved in a finite volume scheme with the Eddy Dissipation Concept (EDC) model for the turbulence-chemistry interaction and the skeletal KEE mechanism (consisting 17 species and 58 reactions) for the combustion reactions. It was found that mixing in shear layers has a significant impact on the temperature, species and flow fields and could be predicted only with a proper selection of the turbulence levels at the inlet boundaries. Analyzing the minor species reaction path together with the mean and fluctuating temperature fields elucidated the great influence of temperature fluctuations on the net rate of CO and OH production in MILD combustion regime.

1. Introduction

Increasing strict requirements of environmental protection and energy saving made Moderate or Intense Low-oxygen Dilution (MILD) combustion [1] an attractive technology for burning fossil fuels, as it may ensure high combustion efficiencies with low NOx and soot emissions. MILD combustion occurs when reactants are preheated above their self-ignition temperature and when enough inert combustion products are entrained in the reaction region to dilute the flame. As a result, a flame front is no longer identifiable, so that MILD combustion is often denoted as flameless combustion or flameless oxidation [2,3]. The technology is also known as High Temperature Air Combustion (HiTAC) due to the common practice of preheating the oxidizer [4]. In comparison with conventional diffusion or premixed combustion regimes, volumetric enlargement of the reaction zone and more uniform temperature distribution are unique features of MILD combustion [4,5]. It has been shown that the use of this technology can provide, approximately, 30% energy savings and hence CO_2 reduction, 30% reduction in-furnace size and 25% reduction in pollutant emission as compared to current designs [6].

Sabia et al. reported that MILD combustion is a promising technology for low-calorific fuels, high-calorific industrial wastes as well as in presence of hydrogen [7]. Derudi et al. [8] suggested MILD combustion for the utilization in the coke oven gas (COG), which is a by-product of the coke-making process. The use of MILD combustion is also foreseen for gas turbine applications [9], as its stable and noiseless characteristics may avoid the thermo-acoustic instabilities and stresses observed with conventional combustion.

Coelho and Peters simulated a FLOX® furnace, experimentally studied by Özdemir and Peters [10], using the Favre-averaged Navier–Stokes approach [11]. Turbulence-chemistry interaction was treated by means of the steady/unsteady flamelet-pdf approach and the NOx emission was calculated by the Eulerian particle flamelet model in a post-processing stage. They argued that the steady flamelet library was unable to correctly predict the formation of NO, because this is a chemically slow process which is sensitive to the transient effects, while the unsteady flamelet model was able to capture the correct order of magnitude of NOx emissions. The valuable set of measured data provided by IFRF on a semi-industrial furnace operating in flameless conditions [12] resulted in series of publications aiming at investigating several computational approaches. Mancini et al. [13,14] investigated the performance of several combustion models in the RANS approach to predict the in-furnace and exit data measured for the IFRF furnace. They examined the eddy-breakup (EBU) model with a two-step reaction scheme, the eddy dissipation concept model (EDC) with chemical equilibrium and the pdf/mixture fraction model

* Corresponding author. Tel.: +98 021 77240540x2701; fax: +98 021 77240540.
** Corresponding author. Tel.: +39 050 2217840; fax: +39 050 2217866.
E-mail addresses: shahrokh@iust.ac.ir (S. Shahhosseini), l.tognotti@diccism.unipi.it (L. Tognotti).

1359-4311/$ – see front matter © 2011 Elsevier Ltd. All rights reserved.
doi:10.1016/j.applthermaleng.2011.06.007

with and without mixture fraction fluctuations. Apart from small regions within the fuel jet, very good agreement were obtained with all combustion models for the in-furnace and exit temperature, NO and CO emissions. They noticed a strong transient behavior in the weak (fuel) jet [13] and tried to capture it by a reactor network model with GRI-3.0 mechanism and entrainment calculated using RANS model or estimated from the measured data [14]. Their results showed that the failure of a number of RANS models in capturing the structure of weak jet is a result of error in predicting entrainment of fuel into the oxidizer jet and, therefore, is not related to any chemistry sub-models. Recently, Oldenhof et al. provided a set of unique experimental data consisting of 2D velocity measurements and temperature and species profiles on a jet in hot coflow (JHC) burner developed at Delft (DJHC) [15,16]. By recording the flame luminescence with an intensified high-speed camera, they found out that behavior of flame base in DJHC flames is fundamentally different from that of a conventional lifted jet flame in a cold air coflow [15]. They, also, investigated the effect of coflow temperature and jet Reynolds number on the location of flame base using a new definition of flame lift-off height. By analyzing the velocity and temperature data in the near-nozzle region, they showed that the increased entrainment in higher Reynolds number jet, in combination with the positive temperature gradient in radial direction in the near field of the jet, are responsible for decreasing lift-off height [16]. Danon et al. [17] investigated, experimentally and numerically, a FLOX gas turbine combustor operated with various low-calorific value gases. Their investigation showed that the EDC model in conjunction with a three-step global mechanism can reasonably predict the axial profiles of mean temperature and species concentration in the flue gas. While they accurately captured the NO emission at the outlet, large discrepancies were reported between model predictions and measured CO even applying more detailed chemical mechanism. They stated that this discrepancy may arise from the chemical mechanism or the turbulence-chemistry interaction (EDC) model, but did not support it.

Although the concept of MILD combustion has been extensively studied experimentally [5–10,12,15,17–21] and numerically [11,13,14,16,17,22–27,35,40,41], the homogeneous mixing field and slower reaction rates make challenging the accurate modeling of this combustion regime. Basically MILD combustion is characterized by a strong coupling between turbulence and chemistry, occurring at similar timescales [18,23]; thus the turbulence-chemistry interactions should be treated with finite rate approaches.

Among the available experimental data on MILD combustion, the jet in hot coflow (JHC) experiment carried out by Dally et al. [8] has received many attentions because of the number and accuracy of experimental data. The fully characterized mean and fluctuating temperature and species fields for different oxygen levels (3%, 6% and 9%) in the hot coflow stream resulted in a number of publications aiming at the validation of different numerical approaches [24–26].

Kim et al. employed the conditional moment closure (CMC) method to predict flame structure and NO formation of this experiment [24]. A laminar flamelet model was used together with a presumed beta PDF for single mixture fraction to model a three stream mixing problem. The CMC model, however, did not account for differential diffusion effects. Their approach attained some success upstream (z = 30 mm from the burner exit). However, downstream (z = 60 and 120 mm) where interaction between fuel and fresh air becomes more significant, the CMC approach with single mixture fraction model was unable to predict the well-mixed flow field and, therefore, failed to predict all scalars. Moreover, under-prediction of peak flame temperature and OH mass fraction at z = 30 mm was attributed to the poor mixing predictions.

Christo and Dally investigated the performance of various turbulence, combustion and oxidation schemes for predicting the JHC flames [25]. They reported that the solution is sensitive to the turbulent kinetic energy at the fuel inlet, but weakly depends on the turbulence intensity at the hot coflow and shroud air inlets. The fuel inlet mean turbulent kinetic energy estimated from the experiments was reported to be 16 m^2/s^2; however, the authors increased this value up to 60 m^2/s^2 at fuel inlet in the numerical model to improve predictions. Moreover, they found that the best agreement between predictions and measurements could be achieved with a modified constant ($C_{\epsilon 1}$) of the k-ϵ turbulence model. As for the turbulence-chemistry interaction, the modeling results demonstrated that single conserved scalar-based models, i.e. mixture fraction/PDF and flamelet models, even with realistic kinetic mechanisms, are inadequate for modeling of JHC conditions. Christo and Dally obtained successful predictions of species for 9 and 6% O_2 flames by employing the EDC model with a detailed chemistry (GRI-3.0 mechanism consisting of 33 species and 233 reactions) and considering the differential diffusion effects. However, results for 3% O_2 case were less satisfactory. They also concluded that poor performance of the model at the 120 mm axial location could be attributed to the intermittent localized flame extinction which cannot be accounted for by the EDC model. They also noticed that CO levels were predicted higher for the 9% O_2 flame than those of 3% O_2 flame. Inasmuch as higher concentrations of O_2 in the coflow stream are expected to yield higher conversion of CO into CO_2, they concluded that the current chemical path ways of CO conversion into CO_2 do not hold under MILD combustion conditions and a different kinetic mechanism might be required.

Recently, Frassoldati et al. [26] applied the same modeling approach of Christo and Dally [25] with a modification on coflow turbulence level to predict the JHC flames features. They used the EDC model with the kinetic scheme of $CH_4/CO/H_2$ mechanism consisting 48 chemical species and about 600 reactions. They noticed that the amount of oxygen diffusing form the shroud air towards the flame was significantly affected by the coflow turbulence level. Three values for the inlet coflow turbulent kinetic energy (k = 0.04, 0.4 and 2 m^2/s^2) were, therefore, compared. They stated that lower turbulence intensity resulted in lower diffusion of oxygen from the surrounding air to the flame region. Comparing with the 3% O_2 experiment, together with the Dally's recommended turbulence level for the fuel inlet, they suggested a value of 0.4 m^2/s^2 for the turbulent kinetic energy at coflow inlet. Adjusting coflow inlet turbulence intensity substantially improved the computed results of the temperature field close to the burner. However, as it will be shown later, at downstream the predictions deviate largely from the reported values showing that more accurate treatment is still required for the mixing field.

The unconfined JHC flames are complicated in that the turbulent flow field is dependent not only on mixing of three streams of different turbulence levels, but also on the flame cooling, weakened reaction zone and lower reaction rates. Such complex flames demand an accurate resolving of mixing and flow fields as a prerequisite to reasonably predict major and minor combustion products in subsequent steps. In the present study, the numerical modeling of the JHC flames is investigated in detail to identify key modeling issues for predicting temperature and chemical species.

2. Numerical model

The JHC burner, showed in Fig. 1a, consists of a central fuel jet (i.d. = 4.25 mm) through which a hybrid fuel of methane and hydrogen (1–1 by volume) is injected with Reynolds number of 10,000 to the hot oxidizer. A coaxial annulus (i.d. = 82 mm)

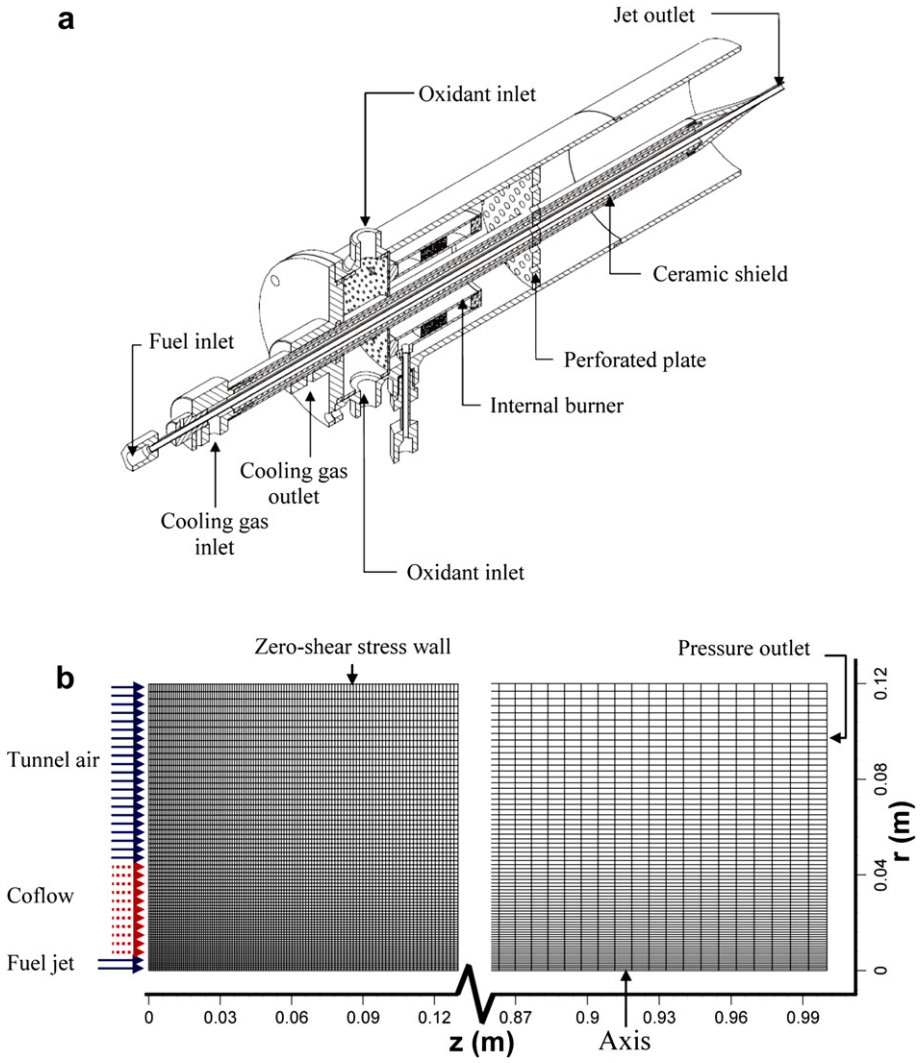

Fig. 1. (a) Burner configuration [20] and (b) Computational domain, mesh grid and boundary conditions.

introduces the hot oxidizer coflow to the reaction zone. The burner was placed inside a wind tunnel. Table 1 shows the operating conditions of all inlet streams for the different case studies. The notations, HM1, HM2, and HM3 refer to the flames with oxygen mass fraction of 3%, 6%, and 9% in the hot coflow stream, respectively. Detailed description of the burner and experimental campaigns can be found elsewhere [20].

2.1. Computational domain and grid

Due to the symmetry of the burner a 2D axisymmetric domain was used. A computational grid with 73×340 cells in radial and axial directions was constructed (see Fig. 1b). It was chosen to use a 1 m long domain in order to cover all the flame length from the jet exit to the far flow field (according to evidences from [22]). The Richardson's extrapolation [28] was employed to evaluate the effect of grid size on the numerical results. The cold-flow center line velocity profile predicted by four different structured grids of 13, 20, 25 and 33 k elements was evaluated. The grid with 25 k cells was found to be the optimum grid, as it provided the smallest relative discretization error (RDE_{ij}) between two subsequent i and j grids.

As can be observed from Fig. 1b, the thicknesses of the walls between the central fuel jet and the coflow and between the coflow and the tunnel air have been neglected. In fact, these thicknesses are of 0.2 and 2.8 mm, respectively. Preliminary simulations were performed in order to assess the effect of such thicknesses on the predictions (results not shown here) but no improvements were

Table 1
Operating conditions for different JHC flames (compositions are as mass fractions) [20].

	Fuel jet				Oxidant coflow					Tunnel air		
Flame	Q (kg/s)	T (K)	CH_4 (%)	H_2 (%)	u (m/s)	T(K)	O_2 (%)	H_2O (%)	CO_2 (%)	u (m/s)	T (K)	O_2 (%)
HM1	3.12e-4	305	88	11	3.2	1300	3	6.5	5.5	3.2	294	23.2
HM2	3.12e-4	305	88	11	3.2	1300	6	6.5	5.5	3.2	294	23.2
HM3	3.12e-4	305	88	11	3.2	1300	9	6.5	5.5	3.2	294	23.2

achieved. Therefore, the computational domain without wall thicknesses (as shown in Fig. 1b) was selected for further studies as it contained much less elements, so that to make simulations more affordable.

2.2. Boundary conditions

Uniform velocity and composition profiles, presented in Table 1, are given to the unmixed fuel jet, coflow oxidizer and tunnel air inlet streams. Combustion products and part of non-reacted tunnel air exhaust through the exit which was treated as a pressure outlet. A zero-shear stress wall was adopted to the side boundary, instead of a more realistic pressure inlet/outlet conditions. However, as the tunnel air was considered wide enough this boundary condition did not affect the flame structure, while largely improved the convergence and simulation time. Preliminary simulations were devoted to validate this aspect. It has been reported, that the inlet turbulent kinetic energy has a great influence on the accuracy of numerical results [25,26]. Therefore, significant effort was assigned to analyze this issue.

2.3. Physical model

The steady-state Favre-Averaged Navier–Stokes (FANS) equations were solved in a finite volume scheme using the commercial CFD code FLUENT 6.3 by ANSYS Inc [30]. The Reynolds stress tensor was resolved applying a modified version of the k-ϵ model with the constant $C_{\epsilon 1}$ set to 1.6 (instead of 1.44) to compensate for the round jet/plane jet anomaly [31,32]. For some specific cases simulations were also performed with the Reynolds Stress Model (RSM), but its performance was found unsatisfactory rather than the modified k-ϵ model. In particular, the RSM model failed to predict the radial position of the temperature peak which was systematically shifted towards larger radial coordinates.

The discrete ordinate (DO) method together with the Weighted-Sum-of-Gray-Gases (WSGG) model with coefficients from Smith et al. [33] was employed to solve the radiative transfer equation (RTE). The DO method solved the RTE in 16 different directions across the computational domain.

The interaction between turbulence and chemistry was handled by the EDC model [29]. The skeletal chemical mechanism KEE [34] including 17 species and 58 reversible chemical reactions was used in all simulations. The accuracy of the KEE chemical mechanism to model the MILD combustion regime has already been approved in the literature [27,35].The in-situ adaptive tabulation (ISAT) method of Pope with error tolerance equal to 1e-5 was employed to reduce the computational cost of time integrations [36]. Differential diffusion was taken into account and modeled by calculating binary diffusion coefficients from the kinetic theory and a modification of the Chapman-Enskog formula [37].

Second-order upwind scheme was applied for the space derivatives of the advection terms in all transport equations. The SIMPLE algorithm was employed to handle velocity-pressure coupling in flow field equations [38]. Residuals for all equations were kept lower than 1e-5 as a convergence criterion. The mass-weighted averages of temperature and CO mass fraction were also monitored at the exit plane as another convergence criterion.

3. Results and discussion

3.1. Effect of inlet turbulent kinetic energy

Radial profiles of measured temperature (taken from [20]) for the HM1 flame at two axial locations are plotted in Fig. 2. These temperature profiles show an initial increase, a distinct maximum and a subsequent decay with increasing the radial coordinate r. The initial increase is attributed to the reaction zone and the decay is due to the cooling of coflow stream by the tunnel air. Dashed lines illustrate radial position of the shear layers between fuel jet and coflow (a) and between coflow and tunnel air (b) streams. A smooth change of temperature is clear in both positions revealing a well-mixed region in both shear layers.

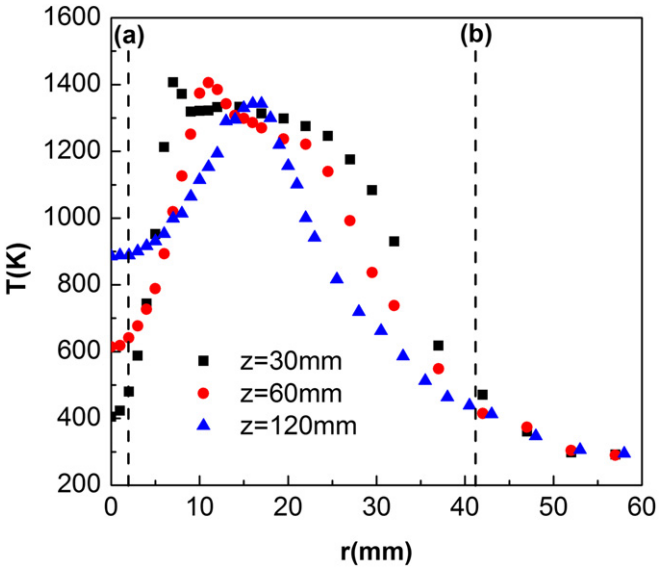

Fig. 2. Radial profiles of measured temperature for HM1 flame at different axial locations [20]. Dashed lines indicate position of shear layers between (a) fuel jet-coflow and (b) coflow-tunnel air at burner exit.

In shear layer flows, the turbulent kinetic energy (TKE) can play an important role in developing the mixing layer [39]. TKE basically represents the mean kinetic energy per unit mass associated with turbulent eddies and can be quantified by the root-mean-square (rms) of velocity fluctuations as $k = 1/2(\overline{u'^2} + \overline{v'^2} + \overline{w'^2})$. Since, the FANS approach is unable to capture the physics of the large eddies and hence the fluctuating velocity field, intensification of TKE at the inlet boundaries could be employed as a numerical tool to induce the turbulent mixing in shear flows. Fig. 3 shows the effect of varying TKE at the inlets on the predicted radial profiles of oxygen mass fraction for the HM1 flame.

For case (a) in Fig. 3, the predicted O_2 mass fractions follow closely the measured values near the center. This is mainly attributed to the increasing TKE at the fuel-jet inlet from 16 m^2/s^2 (measured value) to 60 m^2/s^2 [25]. However, discrepancies are observed apart from the axis. It is worth noting, that for the case (a), the predicted O_2 mass fraction changes sharply at fuel jet coflow and coflow-tunnel air shear layers indicating a poor-mixed flow field in these radial locations comparing with that observed experimentally. Adjusting TKE of the coflow inlet to about 0.43 m^2/s^2 largely improved O_2 distribution on the fuel jet-coflow shear layer as illustrated in Fig. 2b. However, the coflow-tunnel air shear layer still needs treatment. Fig. 3c shows results of the adjusting tunnel air TKE to about 0.15 m^2/s^2. It can be observed that in case (c) the O_2 mass fraction in tunnel-side shear layer is much better predicted than that with the cases (a) and (b). In other words, manipulating inlet turbulence levels using TKE of all three streams resulted in faster mixing of the three inlet streams. The efficient role of inlet TKE adjustment could be supported by inspection of O_2 mass fraction results at further axial distances illustrated in Fig. 4. Particularly, at $z = 120$ mm large deviations of cases (a) and (b) from experimental data emphasizes on the complex flow field in combined shear layer.

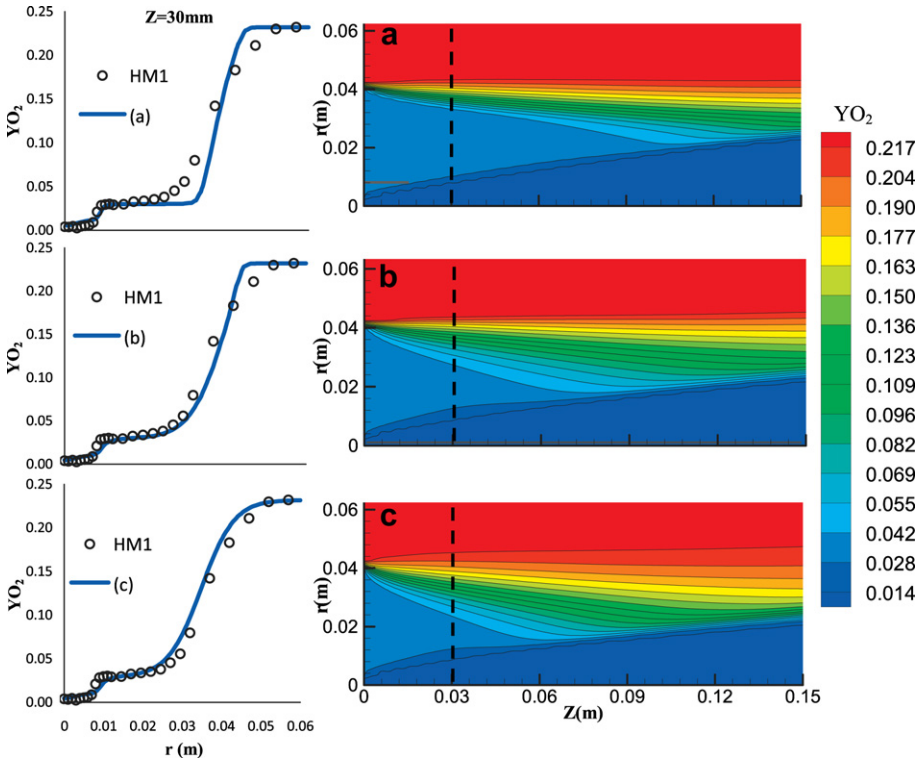

Fig. 3. Distribution of O_2 mass fraction for the HM1 flame predicted by adjusting the turbulent kinetic energy at (a) fuel-jet, (b) fuel-jet, and coflow (c) fuel-jet, coflow and tunnel air inlets.

Similar consideration can be drawn by comparing the predicted temperature profiles with reported values as shown in Fig. 5. All predicted radial profiles of temperature at $z = 30$ and 60 mm are in good agreement with the experiments for what concerns the capturing of the peak flame temperature; however only setting properly the TKE for all inlet streams lead to a good prediction of all temperature profiles. The choice of TKE not only has improved species and temperature predictions close to the burner tip, but also has caused substantial enhancement at downstream ($z = 120$ mm) as shown in Fig. 5c.

The observed over-prediction of peak flame temperature at $z = 120$ mm may arises from different sources. Christo and Dally [25] and Frassoldati et al. [26] reported the localized extinctions and re-ignition phenomena which are not attainable by the adopted EDC model are responsible for over-prediction of peak flame temperature. We believe that in addition to the unattained ignition/extinction phenomena, the EDC model itself tends to slightly over-predict reaction rates in highly diluted and preheated combustion conditions, probably because such conditions are different from those at which the EDC model has been derived. This issue is the subject of further studies on the JHC flames. Very recently, De et al. [40] employed the RANS/EDC approach to simulate the Delft jet in hot coflow (DJHC) flames. They noticed similar over-prediction of peak flame temperature for the DJHC flames and demonstrated that a modification of the EDC constant parameters could result in enhanced predictions of mean temperature field in MILD

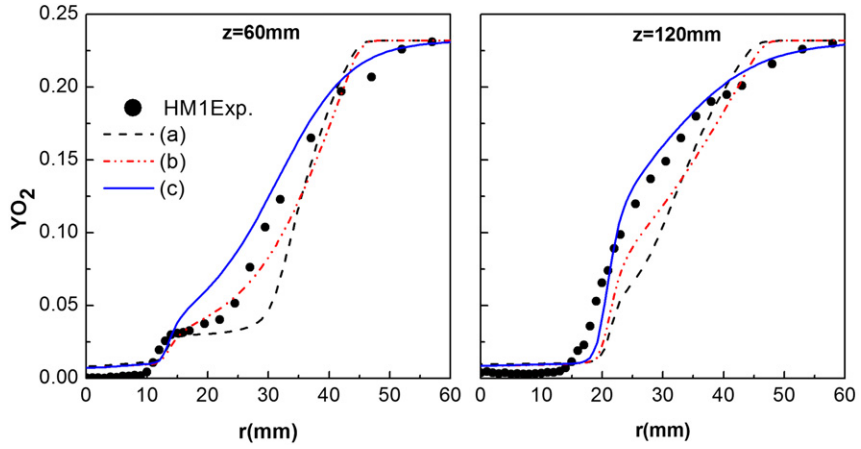

Fig. 4. Comparison between measured radial profiles of O_2 mass fraction for HM1 flame and those predicted by adjusting TKE for (a) fuel-jet, (b) fuel-jet, and coflow and (c) fuel-jet, coflow and tunnel air inlets.

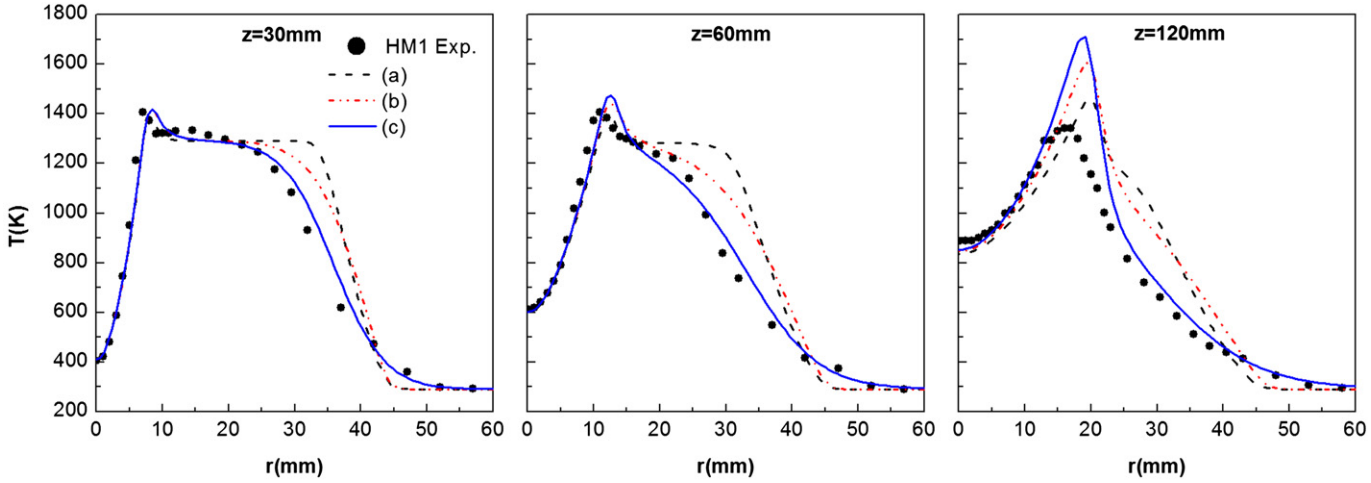

Fig. 5. Comparison between measured radial profiles of temperature for HM1 flame and those predicted by adjusting TKE for (a) fuel-jet, (b) fuel-jet, and coflow and (c) fuel-jet, coflow and tunnel air inlets.

conditions. It can be noticed from Figs. 5–7 that deviation (relative error) of predicted maximum temperature from the experimental values at $z = 120$ mm for HM1, HM2 and HM3 flames were of about 27, 25 and 20%, respectively. It means that the temperature over-prediction by the EDC model goes higher as the dilution increases. This may confirm the impression that the EDC model tends to over-predict reaction rates for diluted combustion conditions.

The same procedure was carried out for HM2 and HM3 flames to accurately predict mixing and temperature fields. Similar to the HM1 flame, the values of 60 and 0.43 m^2/s^2 were selected for the TKE of fuel-jet and coflow inlets and the optimum tunnel air TKE was

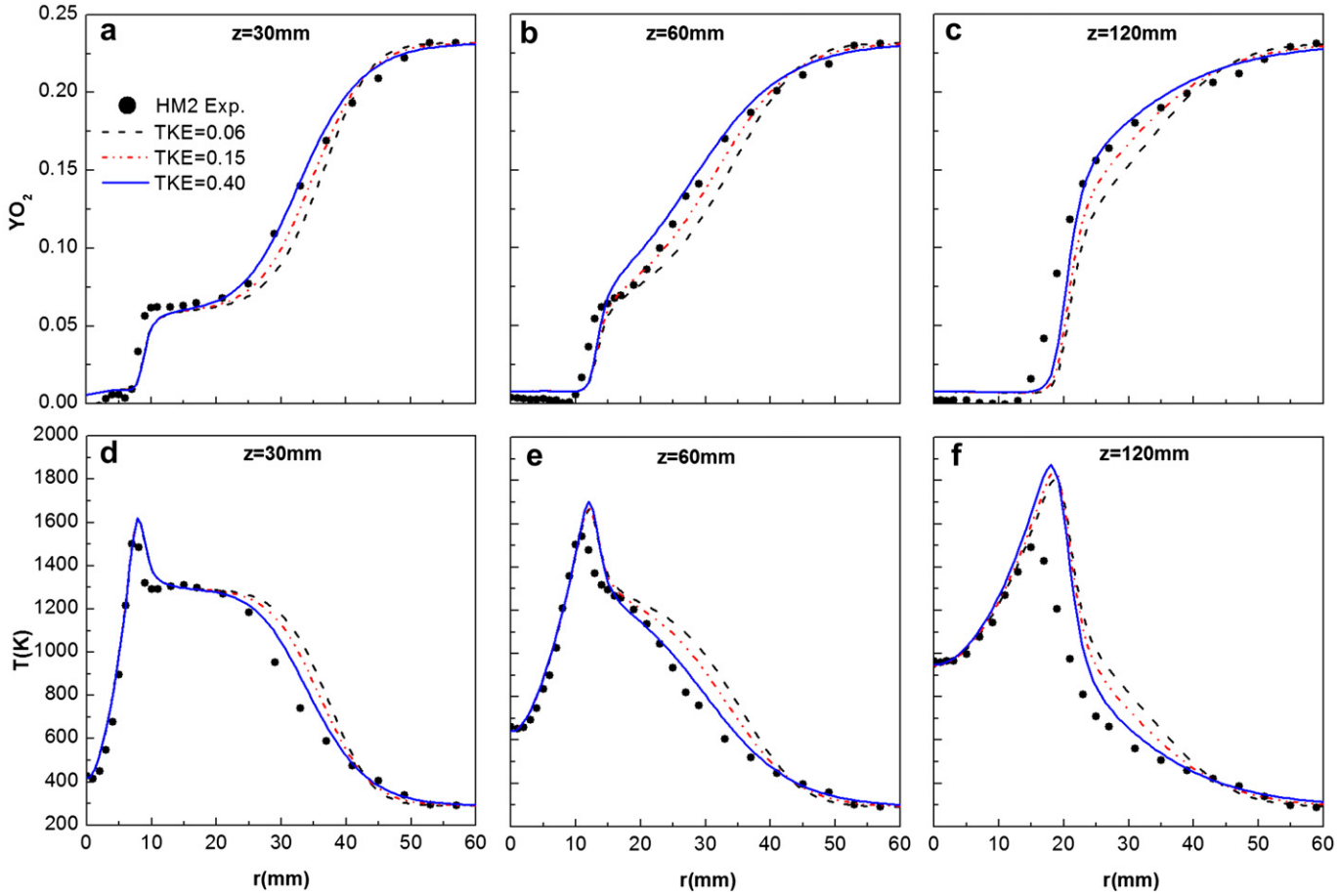

Fig. 6. Comparison between measured profiles of O_2 mass fraction (a–c) and temperature (d–f) for HM2 flame and those predicted with different tunnel air inlet turbulent kinetic energy.

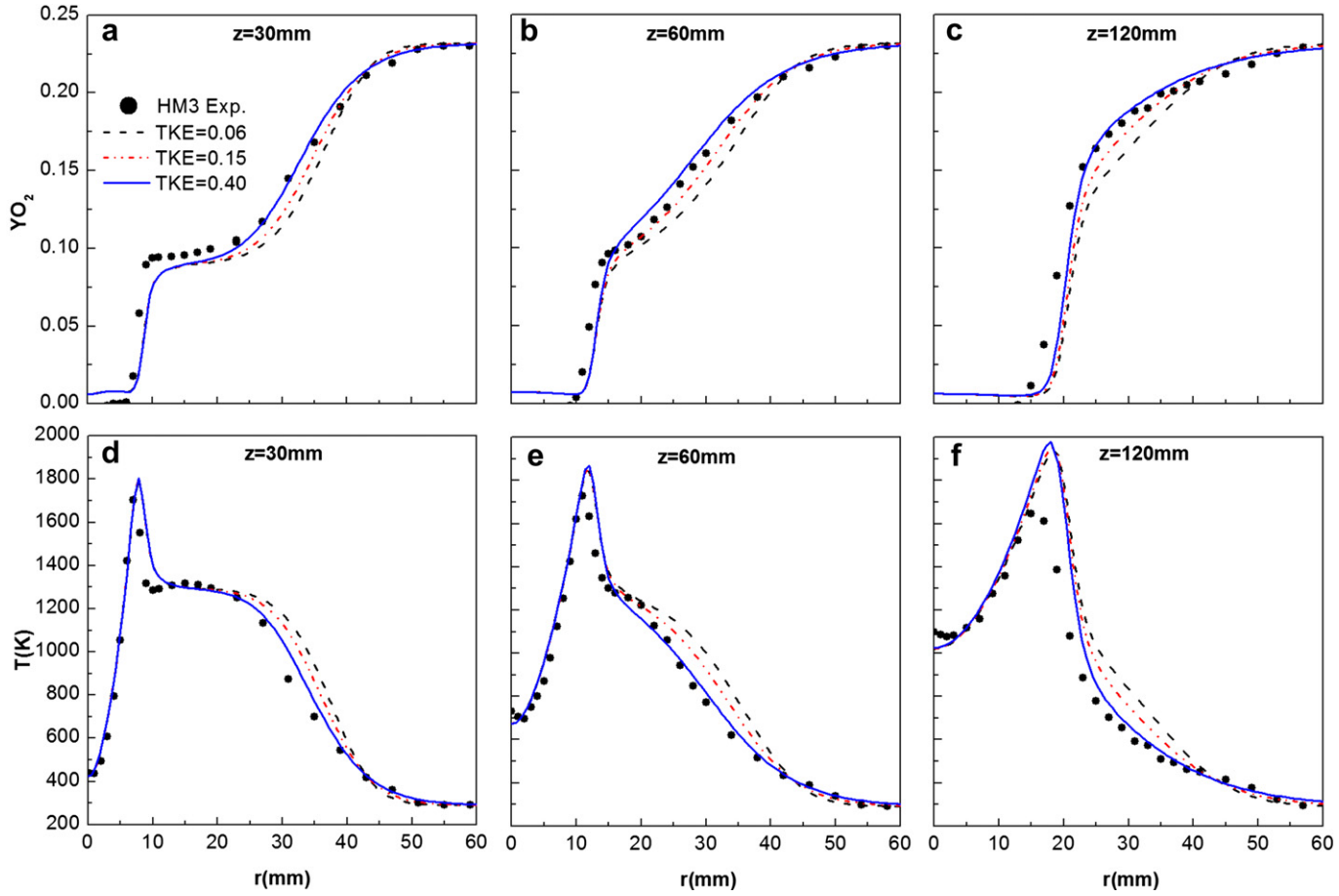

Fig. 7. Comparison between measured profiles of O_2 mass fraction (a–c) and temperature (d–f) for HM3 flame and those predicted with different tunnel air inlet turbulent kinetic energy.

obtained to 0.4 m^2/s^2, through a parametric study, for both HM2 and HM3 flames (according to Figs. 6 and 7). In all cases it is evident that a proper choice of TKE for the inlets affected not only predictions at the upstream, but also at further downstream. Turbulent dissipation rate (ϵ) was estimated from the determined value of TKE for all inlet streams and the corresponding hydraulic diameter (D_h) using $\epsilon = C_\mu^{3/4} k^{3/2} \ell^{-1}$, where, C_μ is an empirical constant equal to 0.09 and ℓ is the turbulence length scale equal to $0.07D_h$.

The quantitative level of agreement between experimental data and predictions is also evaluated through the use of correlation coefficient metrics represented in Table 2 and Table 3 for all flames. The correlation coefficient, defined by Eq. (1), varies between 0 and 1 and denotes the strength of the matching between measured (m) and predicted (p) variables.

$$R^2(m,p) = \frac{C^2(m,p)}{C(m,m)C(p,p)} \quad (1)$$

where C is the covariance matrix. Tables 2 and 3 show the correlation coefficients for oxygen mass fraction and temperature, respectively, obtained with the different tunnel air TKEs.

The strong improvement of predictions obtained by varying the air tunnel turbulent kinetic energy is evident from the correlation coefficients of temperature and oxygen mass fractions. It is also worth nothing that larger correlation coefficients obtained at $z = 120$ mm by using proper TKE at the tunnel air inlet.

Fig. 8 shows the radial distribution of major combustion products (H_2O and CO_2) for the selected tunnel turbulence level of each flame at all axial locations. The predicted H_2O and CO_2 mass fractions are in good agreement with measurements.

It is worth noting, that at the downstream ($z = 120$ mm) both H_2O and CO_2 are over-predicted, in particular for HM1 flame. This may arise from an apparent intense reaction zone predicted by the EDC model at the downstream [40]. Specifically for HM1 flame, it has been reported that reaction zone is weakened and sometimes extinguished at $z = 120$ mm [22]. However, the EDC model does not

Table 2
Correlation coefficient matrix between measured and predicted O_2 mass fraction with different tunnel air TKEs.

	HM1			HM2			HM3		
TKE (m^2/s^2)	0.06	0.15	0.40	0.06	0.15	0.40	0.06	0.15	0.40
$z = 30$ mm	0.995	0.991	0.973	0.984	0.989	0.991	0.980	0.983	0.983
$z = 60$ mm	0.992	0.984	0.951	0.979	0.988	0.987	0.981	0.986	0.986
$z = 120$ mm	0.982	0.986	0.981	0.949	0.966	0.979	0.964	0.976	0.986

Table 3
Correlation coefficient matrix between measured and predicted temperature with different tunnel air TKEs.

	HM1			HM2			HM3		
TKE (m^2/s^2)	0.06	0.15	0.40	0.06	0.15	0.40	0.06	0.15	0.40
$z = 30$ mm	0.971	0.981	0.987	0.958	0.970	0.981	0.962	0.971	0.976
$z = 60$ mm	0.964	0.975	0.964	0.945	0.964	0.973	0.969	0.980	0.980
$z = 120$ mm	0.881	0.902	0.919	0.843	0.875	0.909	0.887	0.917	0.945

account for the dilution effects on the reaction intensity and possible extinction phenomena that can occur in diluted conditions.

3.2. Prediction of minor species

3.2.1. Analysis of carbon monoxide

Predicted and measured radial profiles of carbon monoxide (CO) at three axial locations are illustrated in Fig. 9. Two peaks have been reported in measured values at upstream ($z = 30$ and 60 mm). The peak closer to the burner axis, at about $r = 8$ mm, was predicted quite well for the HM2 (Fig. 9d and e) and HM3 (Fig. 9g and h) flames. The agreement between measured and predicted values in HM1 flame (Fig. 9a and b) is also acceptable. The peak at larger radial coordinate, around $r = 30$ mm was, however, not captured in all simulations.

Analysis of the root mean square (rms) temperatures indicated that temperature fluctuations are maximum (see Fig. 10) in such regions ($r = 8$ and 30 mm) which correspond to the fuel jet-coflow and coflow-tunnel air shear layers. In Fig. 10 dashed lines (a), (c) and (d) represent the location of fuel jet-coflow, coflow-tunnel air and combined shear layers, respectively. The EDC model accounts for temperature fluctuations via a temperature difference between fine structures (T^*) and local mean ($\overline{T}$) temperatures [29]. According to Eq. (2) in the EDC model this temperature difference computes based on the heat of combustion (ΔH_r) generated in reaction zone.

$$\Delta T = T^* - \overline{T} = \frac{\Delta H_r \cdot \overline{c}_{\min}}{\overline{\rho} \cdot C_P} \tag{2}$$

where, $\overline{c}_{\min}$ is the smallest of mean molar concentration of fuel ($\overline{c}_{fu}$) and oxidizer ($\overline{c}_{O_2}/r_{fu}$) and r_{fu} is the stoichiometric O_2 requirement. Such temperature difference is also reported through lines in Fig. 10. Dashed line (b) indicates the location of its maximum: as can be seen, the EDC model showed only one peak of temperature difference in each radial directions which, based on Eq. (2),

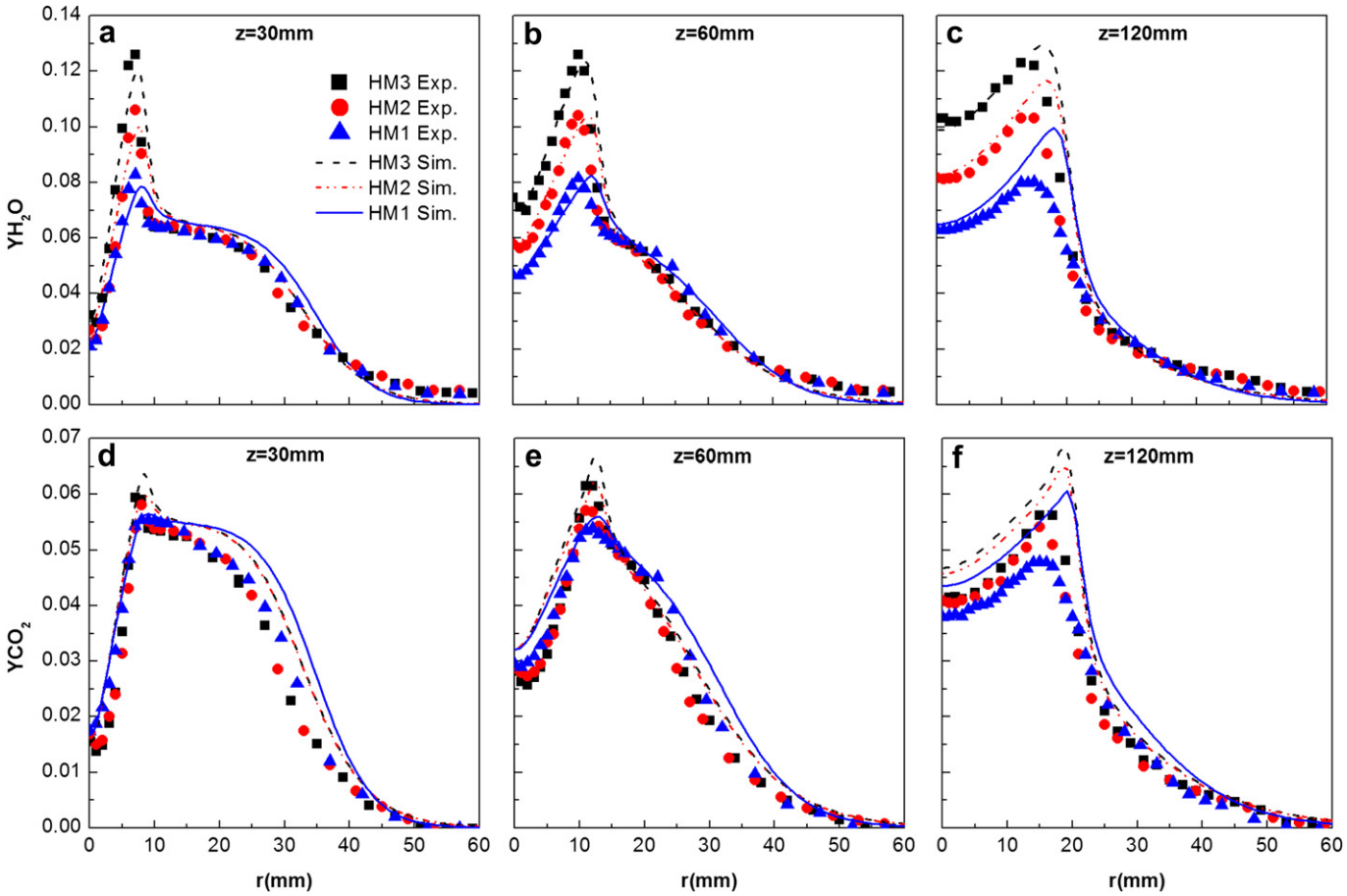

Fig. 8. Comparison between measured and predicted radial profiles of major species (CO_2, H_2O) at different axial locations for HM1, HM2 and HM3 flames. TKE adjusted for all inlet streams.

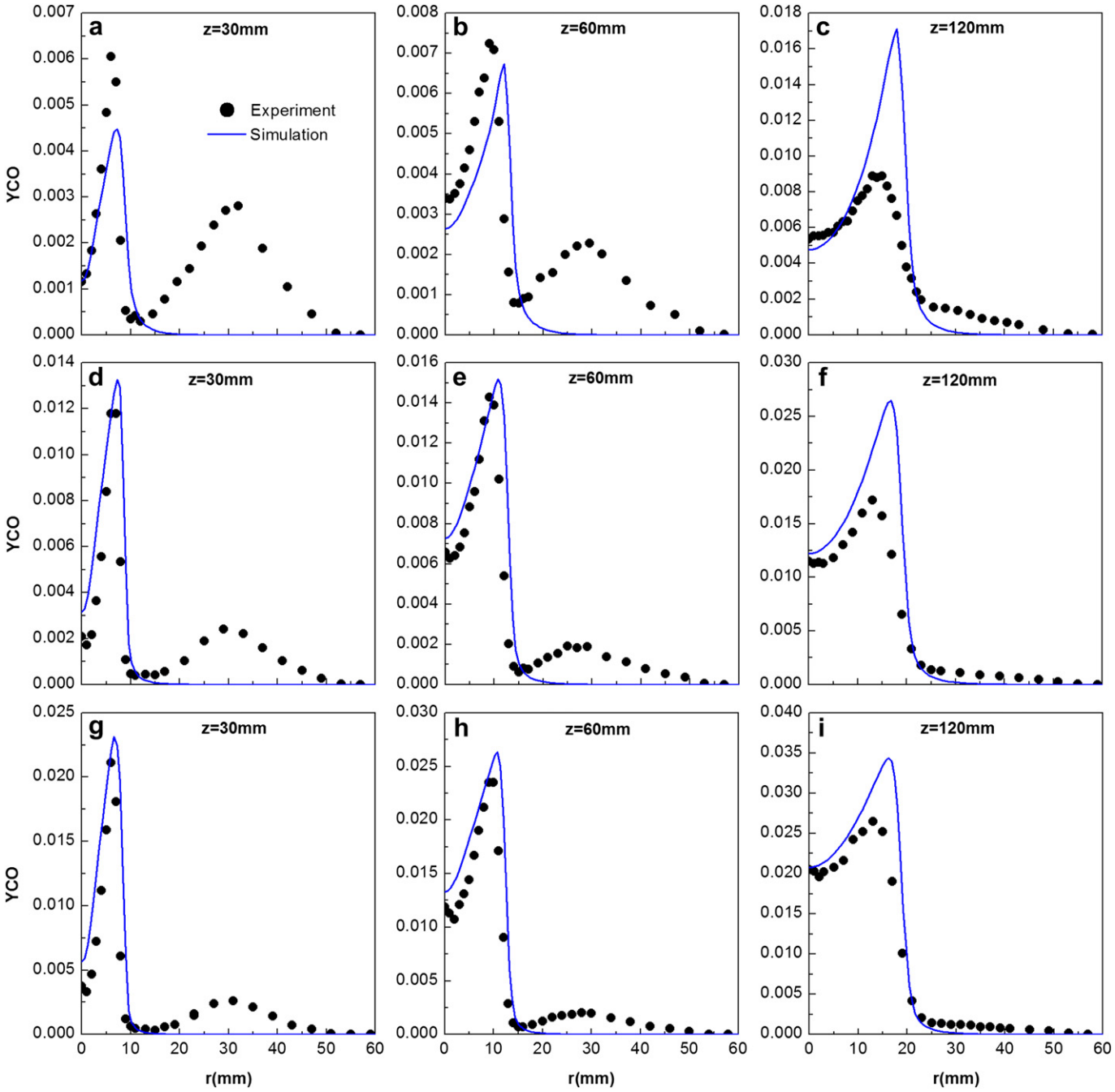

Fig. 9. Comparison between predicted and measured profiles of CO mass fraction for HM1 (a–c), HM2 (d–f) and HM3 (g–i) flames.

corresponds to the flame reaction zone. However, the presence of shear layers in this experiment resulted in higher temperature fluctuations originated from fluctuating mixing field. This, practically, results in spots of high temperature which subsequently lead to higher production of CO. To elucidate the effect of temperature fluctuations on the net rate of CO production, reaction path of CO production/consumption in the KEE mechanism was investigated. Table 4 presents all the reactions in the KEE mechanism which contributes in CO production/consumption. Fig. 11a illustrates those temperature dependent reaction rates of CO presented in Table 4. Dashed lines (1)–(3) correspond to the temperature level of the fuel jet-coflow, coflow-tunnel air and combined shear layers, respectively, as indicated in Fig. 11b. It is worth noting, that the produced CO takes its origin from two major path ways. First one is the oxidation of methane to formaldehyde (CH_2O) which sequentially forms CO by hydrogenation, oxidation or H-abstraction of CH, CH_2 and HCO. This involves reactions number 1–11 in Table 4. The second path is the direct conversion of CO_2 to CO comprising reactions number 12–15 in Table 4. It can be observed from Fig. 11, that among all kinetics, reaction no. 35 ($CO + O + M = CO_2 + M$) is the key mechanism which controls the net production of CO. This reaction could be partly responsible for the first peak of CO mass fraction at upstream ($z = 30$ and 60 mm) and mostly involved in the production of CO at downstream. It arises from the fact that the peak temperature of all flames at upstream is not high enough for which thermal dissociation of CO_2 to CO occur. However, at

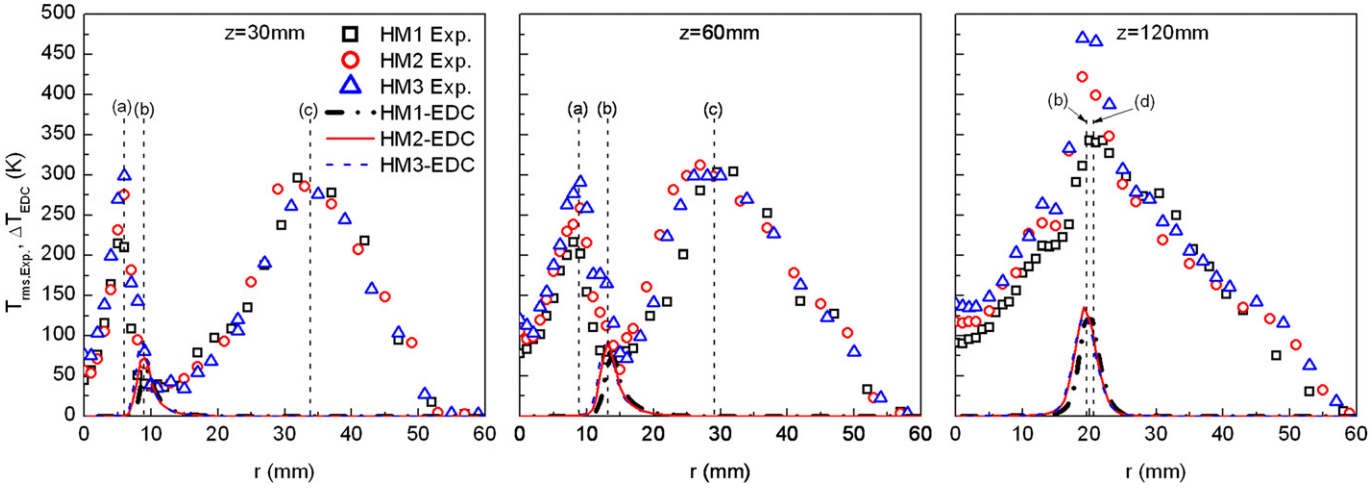

Fig. 10. Radial distribution of measured temperature fluctuations in JHC burner [20] and difference between fine structure and local mean temperature predicted by the EDC model. Dashed lines (a), (c) and (d) represent the location of fuel jet-coflow, coflow-tunnel air and combined shear layers, respectively. Dashed line (b) indicates the location of reaction zone predicted by the EDC model.

downstream higher temperature in reaction zone shifts the CO production from CH_4 origin to the CO_2 decomposition. For the second peak of CO at upstream (Fig. 9a, b, d, e, g and h) the situation is more complex. In one hand, there is no CH_4 in the coflow stream. So, none of reactions number 1–11 in Table 4 could be responsible for this peak. On the other hand, low temperature level in the coflow-tunnel air shear layer hampered the production of CO via CO_2 decomposition (Rn. 35). Therefore, the only candidates for producing CO in the coflow-tunnel air shear layer are reactions number 36–38. In fact, the presence of CO_2 in the coflow stream has activated this route. To clarify this phenomenon, the chemical reaction rates contributed in CO production in the outer shear layer (Rn. 36–38) are plotted vs. temperature in Fig. 12. As can be seen, the contribution of reaction 37 ($CO + O_2 = CO_2 + O$) in CO production is negligible against reactions 36 and 38. It is clear that reaction 36 ($CO + OH = CO_2 + H$) is the dominant reaction in CO production, particularly around the coflow-tunnel air shear layer. This has been confirmed, previously, by Park et al. [41] who investigated the effects of CO_2 addition to oxidizer and fuel streams on the structure of H_2–O_2 counter flow diffusion flame. By analyzing CO mole production rates of several contributed reactions, they showed that the reaction $CO + OH = CO_2 + H$ is, primarily, responsible for CO production under the effect of CO_2 addition to both fuel and oxidizer streams. As can be seen in Fig. 12, the second peak of CO observed at upstream shares interesting features between all JHC flames. Unlike the first CO peak, the second peak has a constant value, 0.0030 at $z = 30$ mm and 0.0025 at $z = 60$ mm, in all HM1, HM2 and HM3 flames. This shows the independence of this peak from oxygen level and is another confirmation for rolling out the contribution of reaction no. 37 from CO production in the coflow-tunnel air shear layer. In addition, since all JHC flames has the same amount of CO_2 in the coflow stream ($Y_{CO_2} = 0.055$) similar amount of CO production for all of them justified the dominant contribution of reaction 36 ($CO + OH = CO_2 + H$) in generation of second CO peak. Actually, the H atom, consumed in Rn. 36, is originated from dissociation of equally added amount of H_2O to the coflow streams of all JHC flames ($Y_{H_2O} = 0.065$), which produced the chain carrier radicals (H, O and OH). Briefly, it can be concluded that equal amount of added CO_2 and H_2O to the coflow stream of all JHC flames activated another CO production route (Rn. 36) in the outer shear layer which is the main source of the second CO peak observed at upstream.

Notwithstanding that the second CO peak was measured at upstream, it was not captured in all simulations as shown in Fig. 9. According to Fig. 12 the reaction number 36, which is responsible for CO production in the outer shear layer, is more sensitive to the temperature fluctuations around 800 K (coflow-tunnel air shear layer) rather than 1600 K (fuel jet-coflow shear layer). Comparing Figs. 10 and 11 indicates that the rms temperature peak closer to the axis, related to the fuel jet-coflow shear layer, has no significant influence on the net rate of CO production. Indeed, almost accurate results were achieved for the first CO mass fraction peak in Fig. 9 at $z = 30$ and 60 mm only through the accurate prediction of the mean temperature field. However, comparing Figs. 10 and 12, shows that the rms temperature peak at larger radial coordinates (at $z = 30$ and 60 mm in Fig. 10), related to the coflow-tunnel air shear layer, can largely influence the net rate of CO production as it occurs at mean temperature around 800 K (Fig. 12) where the reaction no. 36 shows a clear ascending trend. Since, these fluctuations originated from fluctuating mixing field and cannot be taken into account by the adopted FANS/EDC approach the second CO peak at $z = 30$ and 60 mm in Fig. 9, was not captured for all flames. Accordingly, the only peak of the rms temperature at $z = 120$ mm, depicted in Fig. 10, has no influence on the net rate of

Table 4
CO reaction path in the KEE mechanism. Rate constants are in $AT^b\exp(-E/RT)$ format. Units are mole, cm, s, K and cal/mol [34].

No.	Reaction no. in the KEE mechanism	Reaction	A	b	E
1	14	$CH + O = CO + H$	5.70E+13	0	0
2	16	$CH + CO_2 = HCO + CO$	3.40E+12	0	690
3	17	$CH_2 + CO_2 = CH_2O + CO$	1.10E+11	0	1000
4	18	$CH_2 + O = CO + H + H$	3.00E+13	0	0
5	19	$CH_2 + O = CO + H_2$	5.00E+13	0	0
6	23	$CH_2 + O_2 = CO + H_2O$	1.90E+10	0	−1000
7	24	$CH_2 + O_2 = CO + OH + H$	8.60E+10	0	−500
8	30	$HCO + OH = CO + H_2O$	5.00E+12	0	0
9	31	$HCO + M = H + CO + M$	1.60E+14	0	14,700
10	32	$HCO + H = CO + H_2$	4.00E+13	0	0
11	34	$HCO + O_2 = HO_2 + CO$	3.30E+13	−0.4	0
12	35	$CO + O + M = CO_2 + M$	3.20E+13	0	−4200
13	36	$CO + OH = CO_2 + H$	1.51E+07	1.3	−758
14	37	$CO + O_2 = CO_2 + O$	1.60E+13	0	41,000
15	38	$HO_2 + CO = CO_2 + OH$	5.80E+13	0	22,934

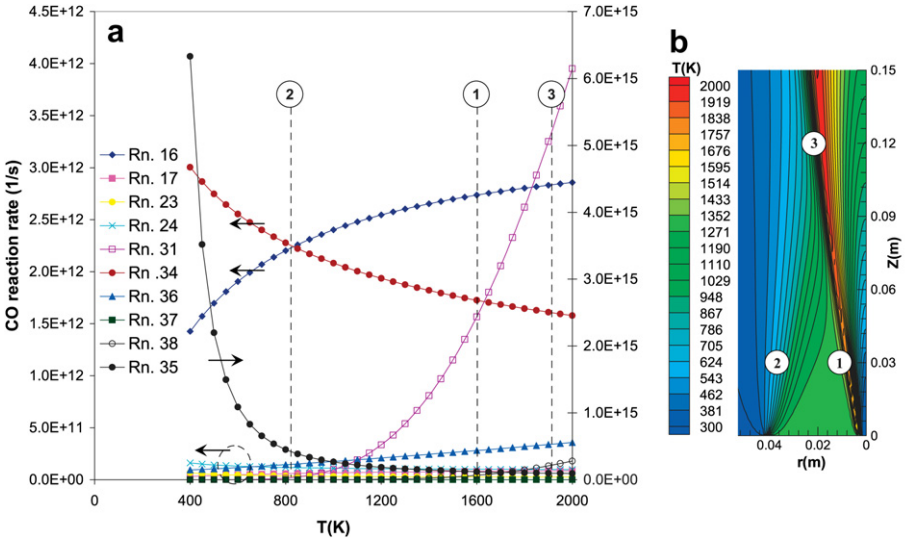

Fig. 11. (a) Temperature dependent reaction paths involving CO in the KEE mechanism. Dashed lines represent temperature level for the 1. Fuel jet-coflow, 2. Coflow-tunnel air and 3. Combined shear layers. (b) Temperature field predicted for HM3 flame.

CO production in Fig. 11 as it occurred in the combined shear layer of three streams at temperature around 1900 K where the reaction no. 35 ($CO + O + M = CO_2 + M$) shows a quite uniform manner. Therefore, the large over-prediction of CO at downstream (depicted in Fig. 9c, f and i) is mainly attributed to the over-prediction of mean temperature field illustrated in Figs. 5, 6 and 7. It is worth noting, that the temperature level of the fuel jet-coflow shear layer decreases for the HM2 and HM1 flames with respect to the HM3 flame, resulting in a small shift of the dashed line (1) in Fig. 11a to the left-hand side. Even considering such a shift in Fig. 11a, temperature fluctuations of the fuel jet-coflow shear layer do not affect CO production in this region, as those temperature levels for HM1 and HM2 flames are, still, located in the flat region of the curve representing reaction no. 35. Therefore, the first CO peak at the upstream of HM1 and HM2 flames was not affected by the temperature fluctuations and can be predicted reasonably by accurate prediction of mean temperature field as illustrated in Fig. 9a, b, d and e.

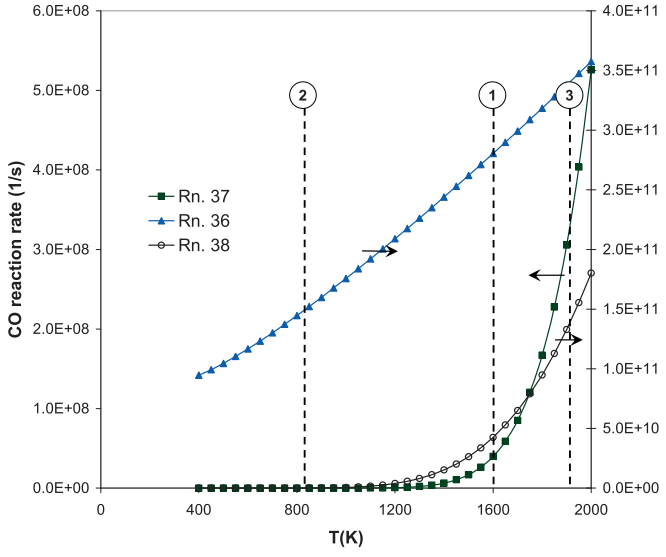

Fig. 12. Chemical reactions of the KEE mechanism involved in CO production in coflow-tunnel air shear layer. Dashed lines represent temperature level for the 1. Fuel jet-coflow, 2. Coflow-tunnel air and 3. Combined shear layers.

It is interesting to note, that the role of temperature fluctuations on the prediction of CO mass fraction increases as the combustion regime switches from flame-like conditions (HM3) to MILD combustion mode (HM1). In the other words, the reduced mean temperature field in HM1 flame highlights the impact of fluctuating temperature on CO production as can be drawn by comparing the contribution of second CO peak in Fig. 9a and b with that in Fig. 9g and h.

3.2.2. Analysis of hydroxyl radical

Fig. 13 compares the predicted and reported mass fractions of hydroxyl radical (OH). The OH is generally considered as a flame marker, thus the location of peak flame represented by the OH peaks, is accurately captured by the numerical model. At first glance it seems that the maximum amount of OH, representing the reaction intensity, was also accurately predicted at upstream especially for HM3 flame. To elucidate the reason, reaction rates of all chemical kinetics involving OH in the KEE mechanism were plotted against temperature in Fig. 14. Table 5 shows these reactions together with their constant parameters. It can be seen from Fig. 14, that the rate of OH production/consumption is mainly controlled by reaction no. 52 ($H + OH + M = H_2O + M$). The reported mean peak temperature in all JHC flames varies between 1343 K (HM1 at $z = 120$ mm) to 1727 K (HM3 at $z = 60$ mm) indicated by the first box in Fig. 14. The second box is obtained by enlarging the first box using the corresponding rms of temperature (maximum 300 K for HM1 at $z = 120$ mm and maximum 250 K for HM3 at $z = 60$ mm) in order to visualize the overall range of temperature fluctuations. Comparing Fig. 12 with Fig. 14 demonstrates that the controlling reaction for the OH production is more sensitive to temperature fluctuation at fuel jet-coflow shear layer (1600 K for HM3 flame in radius around 8 mm) than that for the CO. Hence, temperature fluctuation in fuel jet-coflow shear layer could largely affect prediction of OH. As mentioned in Section 3.2.1, the EDC model computes only temperature fluctuations occurred in reaction zone. However, as can bee seen in Fig. 10, superposition of reaction zone and inner shear layer partly compensated temperature fluctuations

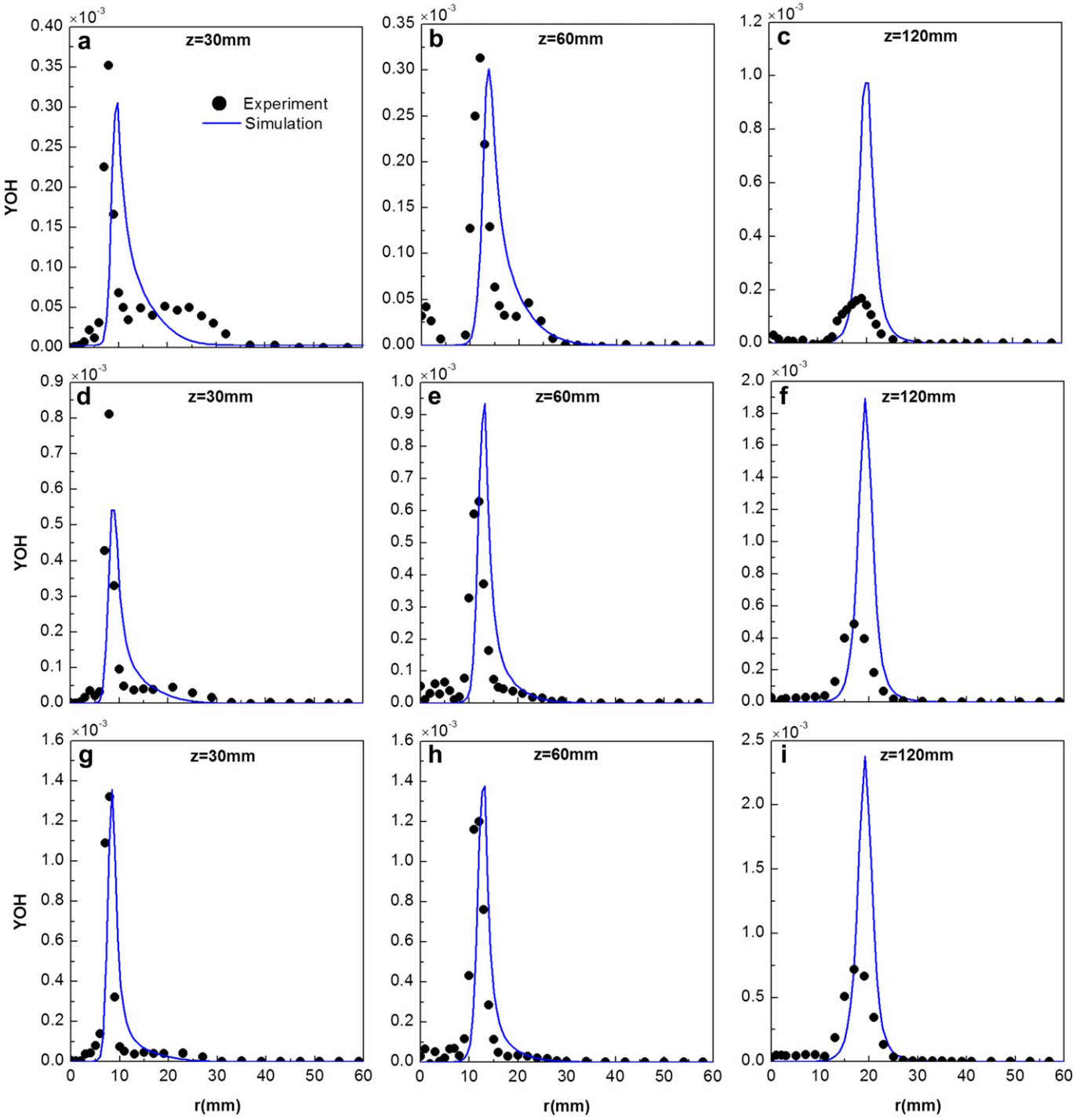

Fig. 13. Comparison between predicted and measured profiles of OH mass fraction for HM1 (a–c), HM2 (d–f) and HM3 (g–i) flames.

originated from fluctuating mixing field. The over-prediction of mean peak temperature illustrated in Fig. 7d and e is another reason for apparently accurate predicted OH mass fraction in HM3 flame. Similar conclusion can be drawn for HM1 and HM2 flames. Temperature fluctuations show a more important role on the OH production for HM1 and HM2 flames (left edge of boxes 1 and 2 in Fig. 14) rather than the HM3 flame. Again, the apparent accuracy obtained in predicted OH mass fraction in HM1 flame (Fig. 13a and b) is attributed to some over-prediction of mean peak temperature (Fig. 5a and b) together with superposition of the reaction zone and inner shear layer which, subsequently, resulted in weakening the significance of mixing-induced temperature fluctuations. Large over-prediction of mean peak temperature at $z = 120$ mm (depicted in Figs. 5, 6 and 7) is clearly responsible for OH over-prediction of all JHC flames at downstream (Fig. 13c, f and i). As a closing remark, it should be noted that the deficiencies observed in prediction of minor species at upstream of JHC flames come from inability of FANS approach on capturing scalar fluctuations and does not attributed to the EDC model. In the ongoing research, large eddy simulation (LES) approach has been employed instead of the FANS

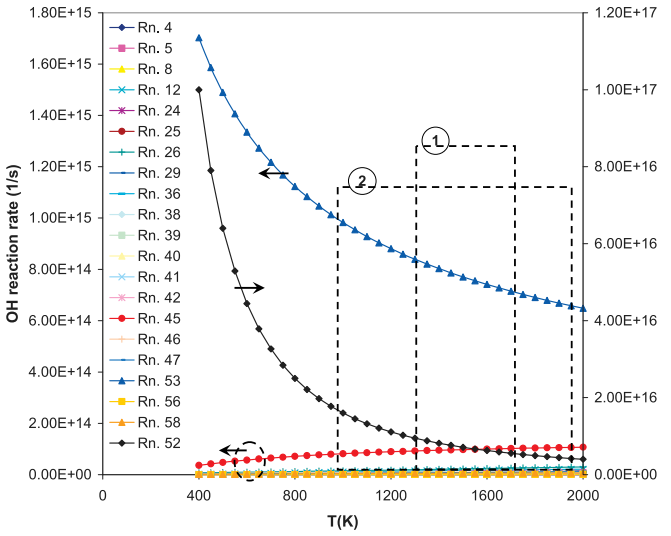

Fig. 14. Temperature dependent reaction path involving OH in the KEE mechanism. The boxes indicate variation limit of (1) mean and (2) instantaneous peak temperature in JHC flames.

Table 5
OH reaction path in the KEE mechanism. Rate constants are in $AT^{b}exp(-E/RT)$ format. Units are mole, cm, s, K and cal/mol [34].

No.	Reaction no. in the KEE mechanism	Reaction	A	b	E
1	4	$CH_4 + O = CH_3 + OH$	1.60E+06	2.36	7400
2	5	$CH_4 + OH = CH_3 + H_2O$	1.60E+06	2.1	2460
3	7	$CH_3 + OH = CH_2O + H_2$	1.00E+12	0	0
4	8	$CH_3 + OH = CH_2 + H_2O$	1.50E+13	0	5000
5	11	$CH_2 + OH = CH_2O + H$	2.50E+13	0	0
6	12	$CH_2 + OH = CH + H_2O$	4.50E+13	0	3000
7	15	$CH + OH = HCO + H$	3.00E+13	0	0
8	24	$CH_2 + O_2 = CO + OH + H$	8.60E+10	0	−500
9	25	$CH_2 + O_2 = HCO + OH$	4.30E+10	0	−500
10	26	$CH_2O + OH = HCO + H_2O$	3.43E+09	1.18	−447
11	29	$CH_2O + O = HCO + OH$	1.81E+13	0	3082
12	30	$HCO + OH = CO + H_2O$	5.00E+12	0	0
13	36	$CO + OH = CO_2 + H$	1.51E+07	1.3	−758
14	38	$HO_2 + CO = CO_2 + OH$	5.80E+13	0	22,934
15	39	$H_2 + O_2 = 2OH$	1.70E+13	0	47,780
16	40	$OH + H_2 = H_2O + H$	1.17E+09	1.3	3626
17	41	$H + O_2 = OH + O$	5.13E+16	−0.816	16,507
18	42	$O + H_2 = OH + H$	1.80E+10	1	8826
19	44	$OH + HO_2 = H_2O + O_2$	7.50E+12	0	0
20	45	$H + HO_2 = 2OH$	1.40E+14	0	1073
21	46	$O + HO_2 = O_2 + OH$	1.40E+13	0	1073
22	47	$2OH = O + H_2O$	6.00E+08	1.3	0
23	52	$H + OH + M = H_2O + M$	1.60E+22	−2	0
24	53	$H + O + M = OH + M$	6.20E+16	−0.6	0
25	56	$H_2O_2 + M = OH + OH + M$	1.30E+17	0	45,500
26	58	$H_2O_2 + OH = H_2O + HO_2$	1.00E+13	0	1800

approach, so that a more in-depth validation on the effect of mixing-induced fluctuations on prediction of minor species in JHC flames can be performed.

4. Conclusion

A numerical study of MILD combustion in a jet in hot coflow (JHC) burner with three different oxygen levels in the hot coflow has been conducted. It was shown that a proper choice of the turbulent kinetic energy at the inlet boundaries is mandatory for capturing the mixing at the shear layers between the three streams, which is a pre-requisite for the accurate prediction of temperature and species mass fractions at both upstream and downstream. Therefore, the knowledge of the inlet turbulence levels is of great importance for jet in hot coflow configurations.

The analysis of minor species such as CO and OH, showed that their production was largely sensitive to the temperature fluctuations especially at upstream of the flame. Reported rms temperatures revealed that maximum temperature fluctuations occur in shear layers between the three inlet streams. Analyzing the CO and OH controlling reactions indicated that temperature fluctuations in coflow-tunnel air shear layer largely affect CO production, while the OH was mainly influenced by those of the coflow-fuel jet shear layer. Consequently, to improve the prediction of minor species in JHC configurations, the temperature fluctuations in shear layers must be resolved directly.

References

[1] A. Cavaliere, M. de Joannon, Mild combustion, Prog. Energy Combust. Sci. 30 (2004) 329–366.
[2] J.A. Wünning, J.G. Wünning, Flameless oxidation to reduce thermal NO formation, Prog. Energy Combust. Sci. 23 (1997) 81–94.
[3] M. Flamme, New combustion systems for gas turbines (NGT), Appl. Thermal Eng. 24 (2004) 1551–1559.
[4] H. Tsuji, A.K. Gupta, T. Hasegawa, M. Katsuki, K. Kishimoto, M. Morita, High Temperature Air Combustion: from Energy Conservation to Pollution Reduction. CRC, 2003.
[5] M. Mortberg, W. Blasiak, A.K. Gupta, Experimental investigation of flow phenomena of a single fuel jet in cross-flow during highly preheated air combustion conditions, J. Eng. Gas Turbines Power 129 (2007) 556–564.
[6] T. Hasegawa, S. Mochida, A.K. Gupta, Development of advanced industrial furnace using highly preheated air combustion, J. Propul. Power 18 (2) (2002) 233–239.
[7] P. Sabia, M. de Joannon, S. Fierro, A. Tregrossi, A. Cavaliere, Hydrogen-enriched methane mild combustion in a well stirred reactor, Exp. Therm. Fluid Sci. 31 (2007) 469–475.
[8] M. Derudi, A. Villani, R. Rota, Sustainability of mild combustion of hydrogen-containing hybrid fuels, Proc. Combust. Inst. 31 (2007) 3393–3400.
[9] C. Duwig, D. Stankovic, L. Fuchs, G. Li, E. Gutmark, Experimental and numerical study of flameless combustion in a model gas turbine combustor, Combust. Sci. Tech. 180 (2008) 279–295.
[10] I.B. Özdemir, N. Peters, Characteristics of the reaction zone in a combustor operating at mild combustion, Exp. Fluids 30 (2001) 683–695.
[11] P.J. Coelho, N. Peters, Numerical simulation of a mild combustion burner, Combut. Flame 124 (2001) 503–518.
[12] R. Weber, S. Orsino, N. Lallemant, A. Verlann, Combustion of natural gas with high-temperature air and large quantities of flue gas, Proc. Combust. Ins 28 (2000) 1315–1321.
[13] M. Mancini, R. Weber, U. Bollettini, Predicting NOx emissions of a burner operated in flameless oxidation mode, Proc. Combust. Ins 29 (2002) 1155–1163.
[14] M. Mancini, P. Schwoppe, R. Weber, S. Orsino, On mathematical modelling of flameless combustion, Combust. Flame 150 (2007) 54–59.
[15] E. Oldenhof, M.J. Tummers, E.H. van Veen, D.J.E.M. Roekaerts, Ignition kernel formation and lift-off behaviour of jet-in-hot-coflow flames, Combust. Flame 156 (6) (2010) 1167–1178.
[16] E. Oldenhof, M.J. Tummers, E.H. van Veen, D.J.E.M. Roekaerts, Role of entrainment in the stabilisation of jet-in-hot-coflow flames, Combust. Flame 158 (8) (2011) 1553–1563.
[17] B. Danon, W. de Jong, D.J.E.M. Roekaerts, Experimental and numerical investigation of a FLOX combustor firing low calorific value gases, Combust. Sci. Technol. 182 (9) (2010) 1261–1278.
[18] T. Plessing, N. Peters, J.G. Wünning, Laser optical investigation of highly preheated combustion with strong exhaust gas recirculation, Twenty-Seventh Symp. (International) Combust. 2 (1998) 3197–3204.
[19] A. Cavigiolo, M.A. Galbiati, A. Effuggi, D. Gelosa, R. Rota, MILD combustion in a laboratory-scale apparatus, Combust. Sci. Technol. 175 (2003) 1347–1367.
[20] B.B. Dally, A.N. Karpetis, R.S. Barlow, Structure of turbulent non-premixed jet flames in a diluted hot coflow, Proc. Combust. Inst. 29 (2002) 1147–1154.
[21] N. Rafidi, W. Blasiak, Heat transfer characteristics of HiTAC heating furnace using regenerative burners, Appl. Thermal Eng. 26 (2006) 2027–2034.
[22] P.R. Medwell, P.A.M. Kalt, B.B. Dally, Simultaneous imaging of OH, formaldehyde, and temperature of turbulent nonpremixed jet flames in a heated and diluted coflow, Combust. Flame 148 (2007) 48–61.
[23] C. Galletti, A. Parente, L. Tognotti, Numerical and experimental investigation of a mild combustion burner, Combust. Flame 151 (2007) 649–664.
[24] S.H. Kim, K.Y. Huh, B.B. Dally, Conditional moment closure modeling of turbulent nonpremixed combustion in diluted hot coflow, Proc. Combust. Inst. 30 (2005) 751–757.

[25] F.C. Christo, B.B. Dally, Modeling turbulent reacting jets issuing into a hot and diluted coflow, Combust. Flame 142 (2005) 117–129.
[26] A. Frassoldati, P. Sharma, A. Cuoci, T. Faravelli, E. Ranzi, Kinetic and fluid dynamics modeling of methane/hydrogen jet flames in diluted coflow, Appl. Thermal Eng. 30 (2010) 376–383.
[27] A. Parente, C. Galletti, L. Tognotti, Effect of combustion model and kinetic mechanism on the mild combustion in an industrial burner fed with hydrogen enriched fuels, Int. J. Hydrogen Energy 33 (2008) 7553–7564.
[28] C.J. Roy, Review of code and solution verification procedures for computational simulation, J. Computational Phys. 205 (2005) 131–156.
[29] B.F. Magnussen, On the structure of turbulence and a generalized eddy dissipation concept for chemical reactions in turbulent flow, 19th AIAA Aerospace Meeting, St. Louis, USA, 1981.
[30] Fluent, The FLUENT 6.3 User's Guide. Fluent Inc, 2005.http://www.fluent.com.
[31] A.P. Morse, Axisymmetric Turbulent Shear Flows With and Without Swirl. Ph.D. thesis. England: London University, 1977.
[32] S.B. Pope, An explanation of the turbulent round jet/plane jet anomaly, AIAA J. 16 (3) (1978) 279–281.
[33] T.F. Smith, Z.F. Shen, J.N. Friedman, Evaluation of coefficients for the weighted sum of gray gases model, J. Heat Transfer 104 (1982) 602–608.
[34] R.W. Bilger, S.H. Starner, R.J. Kee, On reduced mechanisms for methane/air combustion in nonpremixed flames, Combust. Flame 80 (1990) 135–149.
[35] A. Parente, C. Galletti, L. Tognotti, A simplified approach for predicting NO formation in MILD combustion of CH_4–H_2 mixtures, Proc. Comb. Inst. 33 (2011) 3343–3350.
[36] S.B. Pope, Computationally efficient implementation of combustion chemistry using in situ adaptive tabulation, Combust. Theory Model. 1 (1997) 41–63.
[37] H.A. McGee, Molecular Engineering. McGraw-Hill, New York, 1991.
[38] H.K. Versteeg, W. Malalasekera, An Introduction to Computational Fluid Dynamics: The Finite Volume Method. Addison Wesley-Longman, 1995.
[39] E. Costa-Patry, L. Mydlarski, Mixing of two thermal fields emitted from line sources in turbulent channel flow, J. Fluid Mech. 609 (2008) 349–375.
[40] A. De, E. Oldenhof, P. Sathiah, D.J.E.M. Roekaerts, Numerical simulation of Delft-jet-in-hot-coflow (DJHC) flames using the Eddy dissipation concept model for turbulence-chemistry interaction, Flow Turbulence Combust. doi:10.1007/s10494-011-9337-0.
[41] J. Park, D. Hwang, J. Choi, K. Lee, S. Keel, S. Shim, Chemical effects of CO_2 addition to oxidizer and fuel streams on flame structure in H_2–O_2 counterflow diffusion flames, Int. J. Energy Res. 27 (2003) 1205–1220.